Journal of Research and Applications in Mechanical Engineering
ISSN: 2229-2152 (Print); 2697-424x (Online)
(2023) Vol. 11, No. 2, Paper No. JRAME-23-11-014
[DOI: 10.14456/jrame.2023.14]

Research Article

Algorithm for Bone Remodelling Using FEM

S. Luangviset
A. Wisessint*
Department of Mechanical Engineering, Faculty of Engineering, Kasetsart University, Bangkok, Thailand

Received 20 January 2023
Revised 11 May 2023
Accepted 20 May 2023

Abstract:
To repair the injured area and adjust strength to meet the need of the human body, resorption and formation of bones can occur throughout the lifespan depending on the strain factor. An adaptation of the trabecular bone architecture is influenced by load characteristics and outside geometry according to Wolff's law theory. In this paper, a 2D square model of trabecular bone was simulated in finite element analysis (FEA) with varying triangular distribution in compressive load, and the architecture of the trabecular bone was then altered by adding and reducing the element in the direction of the strain based on bone remodelling behavior. Finally, the FEM results showed that the trabecular bone was redesigned and adjusted to have an architecture based on load characteristics and geometry, as described by Wolff's law. This study can be used to predict the architecture and the porosity of trabecular bone.

Keywords: *Bone remodeling, FEM, Wolff's law, Bone architecture*

1. Introduction

Over the time of a person's life, bone resorption and formation can take place in order to repair the injured area and modify strength to satisfy the requirements of the human body. According to Wolff's law theory [1], the trabecular bone architecture can change depending on the load characteristics and external geometry of the bone. Eriksen et al. [2], take the data from histomorphometry research and concludes that bone remodelling behavior has 3 processes: resorption (osteoclast phase depth 19 ± 4.9 μm, mononuclear cells phase depth 49.1 ± 10.2 μm), reversal, and formation (preosteoblast 62.6 ± 12.5 μm) as shown in Fig. 1. Frost's [3] research on the relationship between mechanical force magnitude and the size of bone resorption and formation at the surface, is shown in Table 1. Based on this theory, a lot of research has been done to determine the relationship between adaptation and mechanical loading.

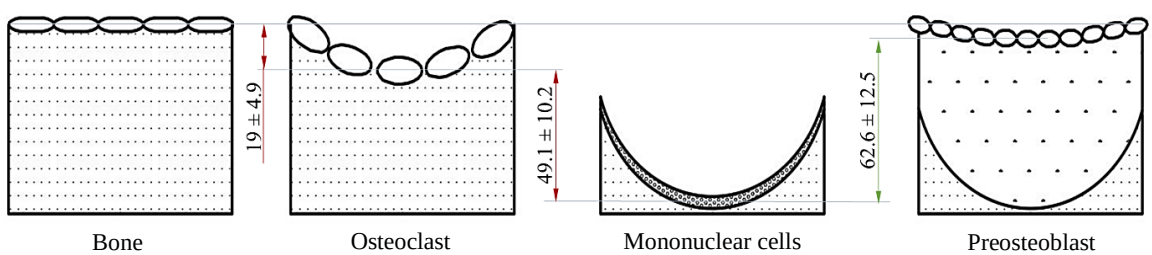

Fig. 1. Trabecular bone remodelling. Osteoclast depth 19 ± 4.9 μm, mononuclear cells depth 49.1 ± 10.2 μm and preosteoblast 62.6 ± 12.5 μm. [2, 4]

* Corresponding author: A. Wisessint
E-mail address: fengapw@ku.ac.th

Table 1: Set Point Values for Bone's Thresholds and Ultimate Strength (Microstrain) [3]

	Microstrain	Action	Mean
MESr	50-100 <	Disuse a bone	Remodelling mechanical thresholds
MESm	> 1000-1500	Build up a bone	Modeling mechanical thresholds
MESp	> 3000	Overload	Pathological mechanical thresholds
Fx	25000	Fracture	Fracture strength

The strain energy density (SED) is the most commonly used variable in the analysis [5] and there are a few other variables [6-8]. But most of them are complicated to analyze and use. In addition, clinical data [2-4] on bone adaptation are researched for diagnosis and treatment purposes in medicine [9].

Therefore, the purpose of this research is to develop a simplified bone remodelling algorithm using finite element method (FEM) for bone remodelling based on clinical data on bone adaptation and Wolff's law theory. The architecture and porosity of trabecular bone can be predicted using the results of this study.

2. Materials and Methods

2.1 Bone Remodelling Algorithm

In the present study, the bone remodelling algorithm was created based on clinical data [2-4] and Wolff's law theory [1] as shown in Fig. 2. Beginning, the FEM model was simulated and analyzed by using the conventional FEM program named Marc/Mentat 2020. The equivalent of total strain (nStrain) at each gauss point of the element (nNumber_Element) was obtained, and then each element was checked to ensure that it was a pore surface of the element. (nNumber_Element_Pore_Surface). Once the pore surface element had been confirmed, the remodelling behavior level [3], as shown in Table 2, was taken into consideration.

As illustrated in Fig. 2, the trabecular bone component of the bone remodelling algorithm was modified following the bone matrix's addition (nStrain>1000) or removal (nStrain<100) on the bone pore's free surface. To simplify the adaptation size from [2, 4], the resorption depth is 68.1 ± 15.1 μm and the formation depth is 62.6 ± 12.5 μm. Distance from Ref. bone surface in the final process is called "Remodelling balance". According to Table 2, the maximum remodelling balance is added +22.1 μm (easily usable: 30 μm), and the minimum is removed -33.1 μm (easily usable: -30 μm).

The FEM bone model in Fig. 3 was constructed using the cortical and trabecular bone components. The cycle (i) of bone remodelling was repeated until the bone matrix modification becomes insignificant (i=6). In contrast to the component of trabecular bone, the cortical bone region was not taken into account in the bone remodelling algorithm.

2.2 Finite Element Model and Boundary Condition

In this paper, Fig. 3 shows a piece of bone with 1 mm of thickness was simulated into 2D FEM model with 9.57 mm x 9.96 mm of the face area. The FEM model was subdivided into 2 components. Above was trabecular bone, with a spongy appearance. This square area was 9.57 mm x 9.57 mm [6, 7, 10, 11] of the face area and had each separation thickness of 0.57 mm [12]. In this region, the bone pores were arranged into a uniform pattern. Below is cortical bone, size 9.57 mm x 0.39 mm. In order to obtain the distributed force behavior of the bone that is similar to the body, and to compare the differences in bone deformation between the lower and higher forces, the triangular distributed load was performed on the top and fixed in y-direction along the bottom and fixed x-direction at the corner of the FEM model. The magnitude of the triangular distributed load is increased until the behavior of the adaptive model changes. The forces applied in this model have magnitudes of 1 and 2 MPa, as shown in Table 3.

Material properties of cortical and cancellous bone were assumed to be homogeneous, isotropic and linear elastic as shown in Table 4.

The model performed a two-dimensional FEA under a plane stress condition with 1 mm thickness. The mesh size was 30μm x 30μm of four-node quadrilateral elements. (Mesh size of the models was optimized to have errors within 1%, a converged mesh size is 30 μm)

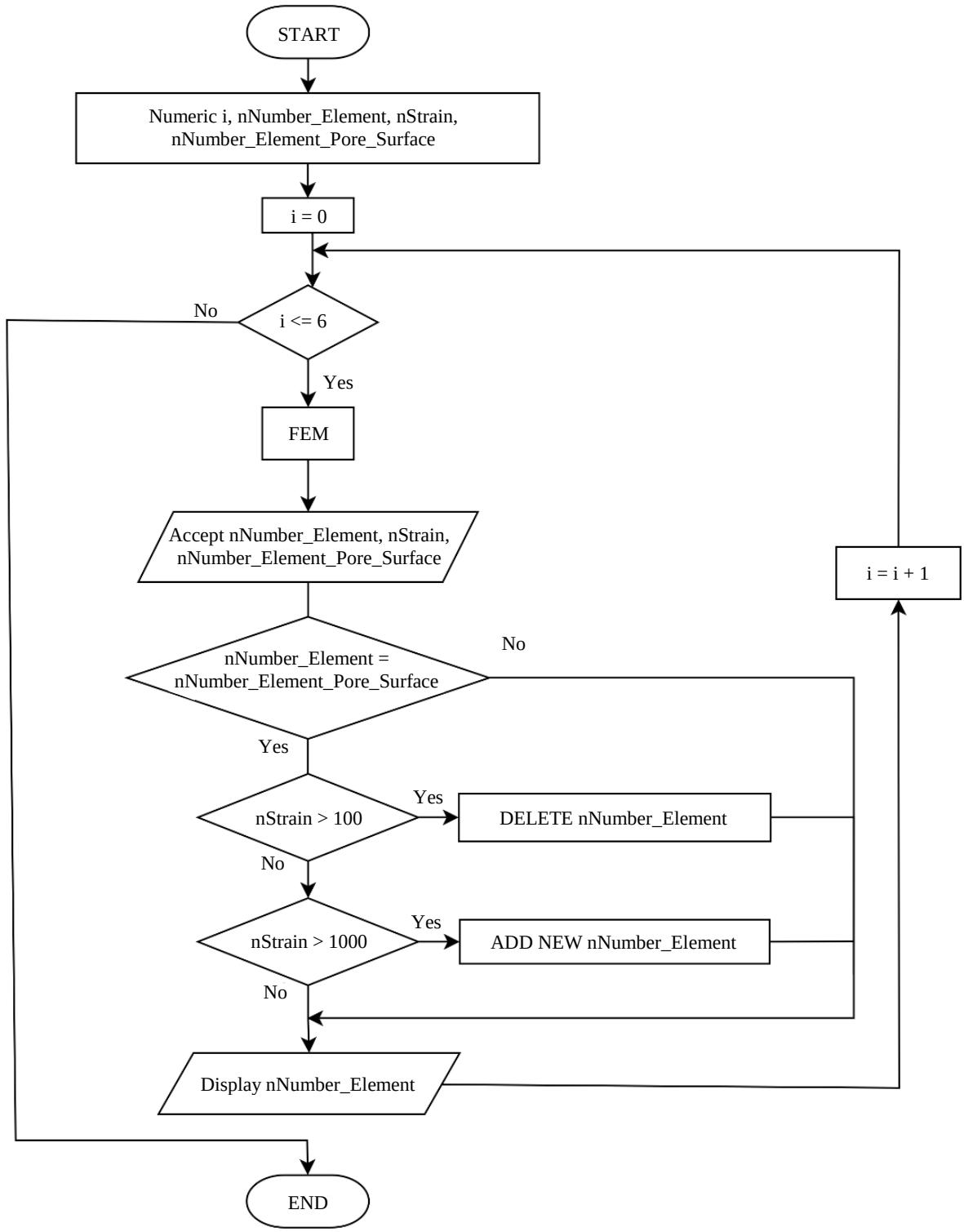

Fig. 2. Bone remodelling algorithm

Table 2: Distance from the reference bone surface in each process. The maximum is shown by the green line, and the minimum is shown by the red line.

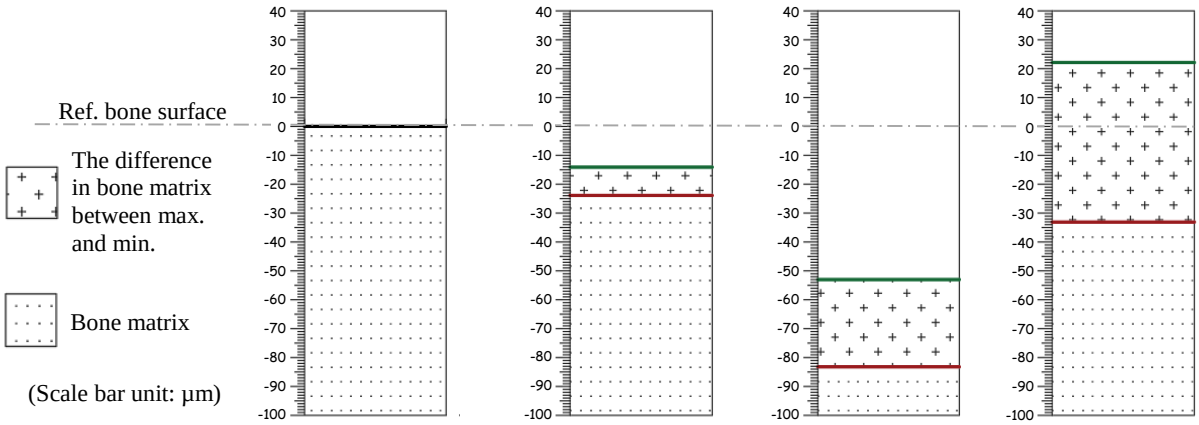

Process	Start	Osteoclast	Mononuclear	Preosteoblast
Depth (μm) [2, 4]		-19 ± 4.9	-49.1 ± 10.2	+62.6 ± 12.5
Distance from Ref. bone surface				
: Maximum (μm)	0	-14.1	-53.0	+22.1
: Minimum(μm)	0	-23.9	-83.2	-33.1

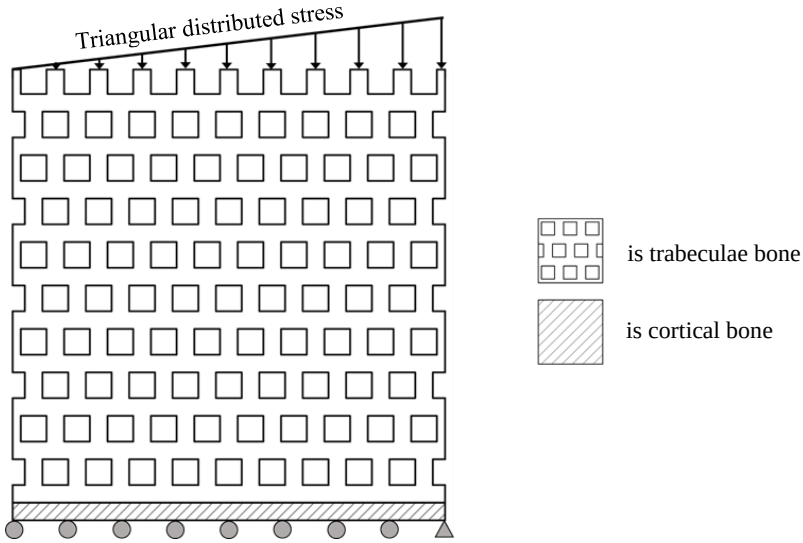

Fig. 3. FEM model and boundary condition [6, 7, 10, 11] triangular distributed stress

Table 3: Load case of each FEM model

Model	Load case	Stress (MPa)
A	triangular distributed	1
B	triangular distributed	2

Table 4: The material properties of bone [11-14]

Bone type	Elastic modulus (GPa)	Poisson's ratio
Cortical Bone	18.6	0.3
Trabecular Bone	10.4	0.3

3. Result and Discussion

Models A and B applied triangular distribution in compressive stress 1 and 2 MPa on the top of the FEM model, respectively. Based on these characteristics of force, the right side of the model exhibit more stress and strain than the left side of both models as shown in Fig. 4. Areas affected by less force have less stress and strain. The region's surface with strains less than 100 microstrain (MESr) has decreased naturally to remove unnecessary parts, which are shown by dark gray regions. The hole surface in this model was simply removed 30 μm at a time, according to Table 2. The balancing region, which is the architecture of the properly stressed bone that causes the bone surface to neither increase nor decrease, is represented by the gray area. And the light gray area has a strain higher than 1000 microstrain (MESm) because it's heavily stressed by a lot of force. Normally, the bone in this region grows new bone by itself to expand the area that can absorb the force. In this model, the hole surface was simply increased by 30 μm at a time as shown in Table 2. Figure 4a clearly demonstrates that most areas are balanced (grey), resorption (dark grey), and less is required for bone formation (light gray) because model A is a low magnitude force. That increasing force is present in model B. As shown in Fig. 4b, it was discovered that there were significantly more areas that needed formation (light gray) than in model A.

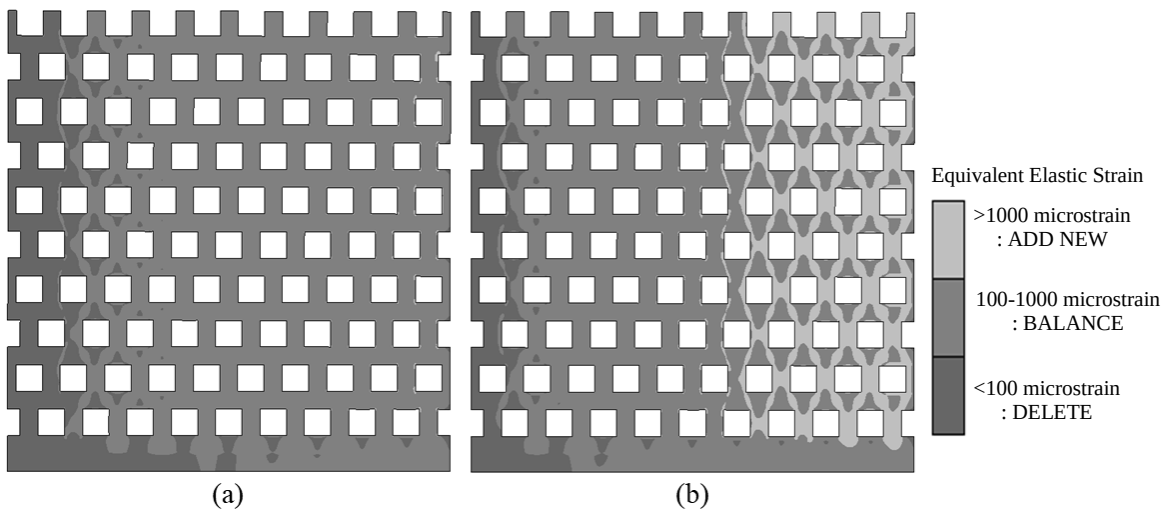

Fig. 4. The equivalent elastic strain at the 1st cycle by FEM program: (a) Model A (b) Model B

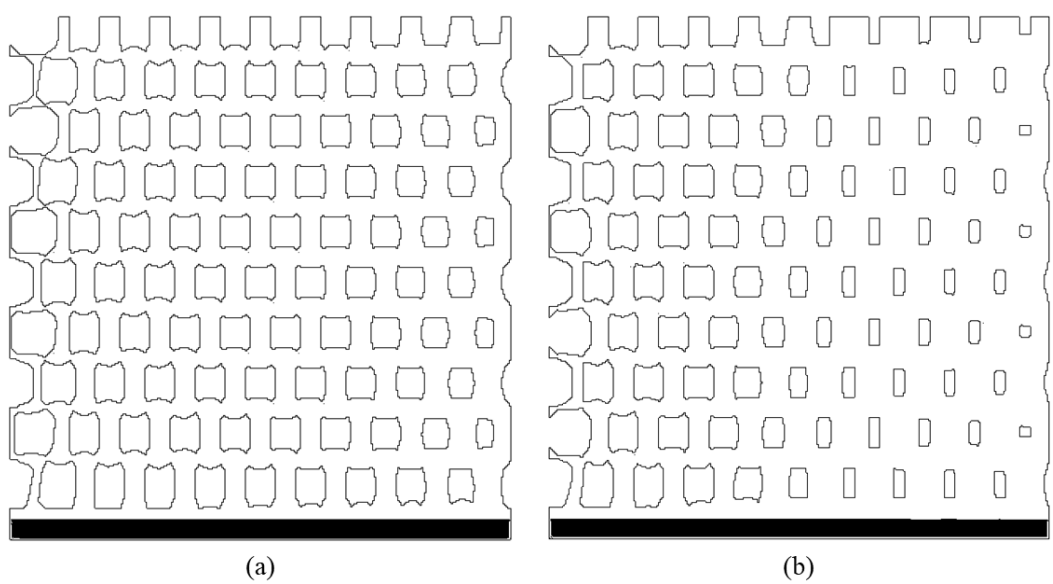

Fig. 5. Bone architecture at the last cycle (loop 6th): (a) Model A (b) Model B

Table 5: Result of bone model

Number of Cycles	Model A		Model B	
	Bone area (mm^2)	**Maximum von mises stress (MPa)**	**Bone area (mm^2)**	**Maximum von mises stress (MPa)**
1	63.0837	32.98	63.0837	66.89
2	62.2548	21.79	64.8026	57.64
3	61.4294	24.29	66.3623	46.97
4	60.6573	20.27	67.8014	39.51
5	59.9359	17.69	69.1073	35.52
6	59.2749	15.08	70.2379	35.42
Reduction of area (%)	93.96		111.34	

If the strain is greater than MESm, the region develops the bone matrix. However, if the strain is less than MESr, the bone reduces, and the adaptation is clearly obvious, as shown in Fig. 5. Both model A and B's bone matrices in Fig. 5 exhibit identical formation and decay patterns. There was a lot of decomposition in the low strain area on the left side of the model, and a lot of bone growth in the high strain area on the right. In Model A (Fig. 5a) and Model B (Fig. 5b), it is apparent that Model A's pore size is bigger than Model B's. Model B's bone matrix and separation thickness are thicker than Model A's, as seen by the model areas in Table 5. This result is consistent with the magnitude of the forces applied.

The large differences between models A and B are apparent, as shown in Table 5, which represents the values of the area and the maximum von mises stress. The area of model A decreases in each loop due to the presence of many regions with a strain less than MESr (less than 100um), in contrast to model B, which has many areas with a higher strain than MESm (more than 100um), as shown in Fig. 4. It illustrates that by using the same model but different values of force and strain, completely different results can be obtained. Whether the area decreases, as in model A, or increases, as in model B, as the number of cycles increases, the maximum von misses stress value always tends to decrease when remodelling is done to achieve the optimal balance of load and geometry, as shown in Table 5.

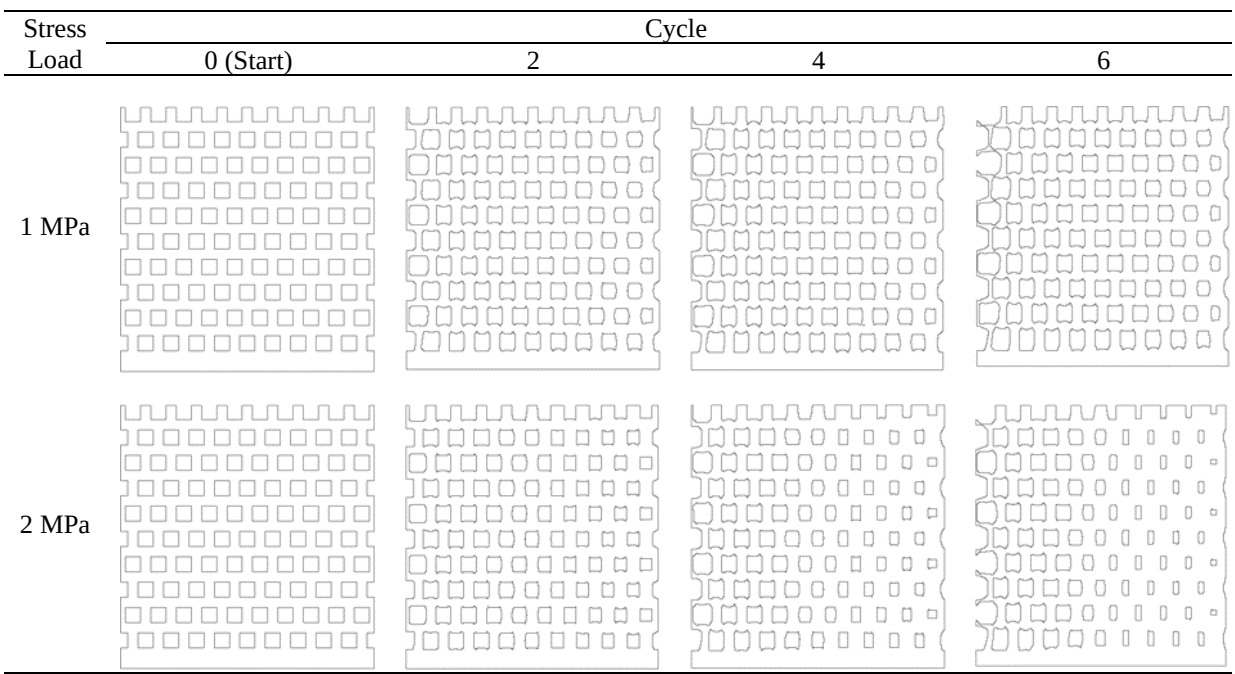

Fig. 6. Bone architecture at cycles 0, 2, 4, and 6.

From the 6 cycles of the bone remodelling algorithm as Fig. 2, the adaptation of the bone matrix around the bone pore in both load cases can be seen in Fig. 6. Since the applied load direction was in the vertical axis and obtained enough level of strain value to build up a bone matrix, the vertical separation thickness was increased, whereas the horizontal separation thickness is broken due to a less stressful region. The separation region rapidly decreases in the low-load zone (left side of the model). As a result, the pores in the nearby bone combine to form a larger cavity. And as the loop grows longer, it tends to merge more pores. The separation area gradually thickens in the highly loaded area (right side of the model), resulting in fewer pores and more bone matrix.

4. Conclusion

The human bone remodelling behavior occurring on the surface of trabecular bone leads to changes in the architecture pattern. This algorithm, simulated from an adaptive process, utilizes strain as a criterion for forming and resorbing the bone matrix. The strain depends on the load characteristics and external geometry, consistent with Wolff's law theory and biological response. The algorithm was applied to the bone model. The trend of trabecular bone architecture has been observed since the first simulation, and it has gradually adapted with each cycle until it reached a steady state. The trend of maximum von Misses stress was similar, with a high value in the initial cycles that gradually decreased in each subsequent cycle until it stabilized, while the bone matrix area could either increase or decrease depending on the strain value that occurred. Because the remodelling algorithm is modeled based on the behavior of human bone resorption and formation, it is easy to understand and simplify the analysis. In the future, this concept may be utilized to predict bone architecture by modeling the characteristics of diverse forces and external shapes.

References

[1] Wolff J. The law of bone remodelling. Berlin: Springer; 1986.

[2] Eriksen EF, Gundersen HJG, Melsen F, Mosekilde L. Reconstruction of the formative site in iliac trabecular bone in 20 normal individuals employing a kinetic model for matrix and mineral apposition. Metab Bone Dis Relat Res. 1984;5(5):243-252.

[3] Frost HM. A 2003 update of bone physiology and Wolff's law for clinicians. Angle Orthod. 2004;74(1):3-15.

[4] Cowin SC. Bone Mechanics Handbook. 2nd ed. Boca Raton: CRC Press; 2001.

[5] Mirulla AI, Pinelli S, Zaffagnini S, Nigrelli V, Ingrassia T, Paolo SD, et al. Numerical simulations on periprosthetic bone remodeling: a systematic review. Comput Methods Programs Biomed. 2021;204:106072.

[6] Fernández JR, García-Aznar JM, Martínez R, Viaño JM. Numerical analysis of a strain-adaptive bone remodelling problem. Comput Methods Appl Mech Eng. 2010;199(23-24):1549-1557.

[7] Baldonedo J, Fernández JR, Segade A. Numerical analysis of a bone remodeling model with damage. Comput Methods Appl Mech Eng. 2020;367:113113.

[8] Jang IG, Kim IY. Computational study on the effect of loading alteration caused by disc degeneration on the trabecular architecture in human lumbar spine. J Biomech. 2010;43(3):492-499.

[9] Park S, Park J, Kang I, Lee H, Noh G. Effects of assessing the bone remodeling process in biomechanical finite element stability evaluations of dental implants. Comput Methods Programs Biomed. 2022;221:106852.

[10] Weinans H, Huiskes R, Grootenboer HJ. The behavior of adaptive bone-remodeling simulation models. J Biomech. 1992;25(12):1425-1441.

[11] Mullender MG, Huiskes R, Weinans H. A physiological approach to the simulation of bone remodeling as a self-organizational control process. J Biomech. 1994;27(12):1389-1394.

[12] Klintström E, Smedby O, Moreno R, Brismar TB. Trabecular bone structure parameters from 3D image processing of clinical multi-slice and cone-beam computed tomography data. Skeletal Radiol. 2014;43(2):197-204.

[13] Wu D, Isaksson P, Ferguson SJ, Persson C. Young's modulus of trabecular bone at the tissue level: a review. Acta Biomater. 2018;78:1-12.

[14] Rho JY, Ashman RB, Turner CH. Young's modulus of trabecular and cortical bone material: ultrasonic and microtensile measurements. J. Biomech. 1993;26(2):111-119.